Monthly Notices
of the
ROYAL ASTRONOMICAL SOCIETY

Mon. Not. R. Astron. Soc. **420,** 2569–2579 (2012) doi:10.1111/j.1365-2966.2011.20228.x

Laboratory far-infrared spectroscopy of terrestrial sulphides to support analysis of cosmic dust spectra

T. Brusentsova,[1] R. E. Peale,[1]⋆ D. Maukonen,[1] P. Figueiredo,[1] G. E. Harlow,[2] D. S. Ebel,[2] A. Nissinboim,[2] K. Sherman[2] and C. M. Lisse[3]

[1]*Department of Physics, University of Central Florida, Orlando, FL 32816, USA*
[2]*American Museum of Natural History, Central Park West at 79th Street, New York, NY 10024, USA*
[3]*The Johns Hopkins University Applied Physics Laboratory, 11100 Johns Hopkins Road, Laurel, MD 20723, USA*

Accepted 2011 November 18. Received 2011 November 17; in original form 2010 December 22

ABSTRACT

As an aid in interpreting data from space far-infrared (far-IR) missions, such as the *Herschel Space Observatory* with its Photodetector Array Camera and Spectrometer, this paper presents spectroscopic studies of selected naturally occurring terrestrial sulphide minerals in the wavelength range 15–250 μm. The data can also be used to support the return from other, both past and planned, IR space missions, such as the *Infrared Space Observatory*, *Spitzer*, *SOFIA*, *SPiCA* and *Millimetron*. In this study, we present far-IR spectra for 11 natural sulphide minerals in the form of dispersed powders of micron particle dimensions. Samples of various sulphides from the American Museum of Natural History mineral collection were selected based on criteria of diversity and potential astrophysical relevancy, based on their identification in *Stardust*, in stratospheric interplanetary dust particle samples, or in meteorites. Mineral species include digenite, galena, alabandite, sphalerite, wurtzite, covellite, pyrrhotite, pyrite, marcasite, chalcopyrite and stibnite. Most of the sulphides examined possess prominent and characteristic features in the far-IR range. Spectra obtained are compared to those available from previous studies. Far-IR peak frequencies and mass absorption coefficient values are tabulated. Effects of particle size distribution, low temperature, and provenance on IR spectra are demonstrated for selected samples.

Key words: line: identification – methods: laboratory – techniques: spectroscopic – circumstellar matter – infrared: general – infrared: stars.

1 INTRODUCTION

Mineralogy of cosmic dust, such as the circumstellar dust of asymptotic giant branch stars, that of young stellar objects (YSOs), planetary nebulae, protoplanetary and debris discs, and comets, may provide information on star and planet formation, petrology of the planetesimals or forming exoplanets, and other important processes. Infrared (IR) emission spectra of such dust collected by space IR missions are useful for the identification of its mineral composition (e.g. Kemper et al. 2002a,b; Chiavassa et al. 2005; Chen et al. 2006; Posch et al. 2006; Mutschke et al. 2008; Henning 2010).

The *far-IR* spectral region (longer than ∼15 μm wavelength) is especially diagnostic of mineral composition, crystal structure, and temperature, and thus, in addition to the *mid-IR* (∼3 to 15 μm), is valuable in the study of cosmic dust mineralogy. Mineral spectra in the far-IR range frequently are rich with prominent and characteristic features, which are attributed to vibrations of the crystal unit cell as a whole. These strongly characteristic bands may differ significantly for polymorphs of the same chemical compound (Nyquist & Kagel 1971; Farmer 1974). Mineral identifications that have been based until recently on one or a few *mid-IR* features can be validated (or refuted) by additional *far-IR* absorption bands (Molster & Waters 2003), as measured in this project.

Far-IR spectroscopy of cosmic dust was started with the *Kuiper Airborne Observatory* (*KAO*) in the 1970s (e.g. Harvey, Thronson & Gatley 1979; Forrest, Houck & McCarthy 1981; Whitcomb et al. 1981; Hanner 1985; Buss et al. 1993; Zhang et al. 1994; Glaccum 1995). Since 1995, far-IR space observations were continued and extended by the *Infrared Space Observatory* (*ISO*) (e.g. Cohen et al. 1999; Crovisier et al. 2000; Chiavassa et al. 2005), *Infrared Astronomical Satellite* (*IRAS*) (e.g. Neugebauer et al. 1984; Nesvorny et al. 2010), *Spitzer Space Telescope* (e.g. Werner et al. 2004; Carpenter et al. 2009), and *AKARI* (also known as *ASTRO-F*, or *IRIS*) (e.g. Murakami et al. 2007). Thus, far-IR spectroscopy has become more and more important for remote sensing of cosmic dust

⋆E-mail: Robert.Peale@ucf.edu

mineralogy (e.g. Henning 2010). Similar efforts are currently underway, including *KAO*'s successor *SOFIA* (Gehrz et al. 2009), and the *Herschel Space Observatory* (Rowan-Robinson 2009; Pilbratt et al. 2010). New far-IR missions are being planned for the next decade, including *SPiCA* (Kerschbaum, Posch & Nowotny 2009; Waters 2009) and *Millimetron* (Wild et al. 2009). Thus, building on the data base of laboratory far-IR spectra of terrestrial mineral analogues, representing a wide range of mineral groups, especially at conditions relevant to those in space (e.g. at cryogenic temperatures), is desirable and timely (Henning 2010).

The mineralogy of various cosmic dust populations is usually determined by comparing their IR emission spectra with laboratory mass absorption coefficient spectra of terrestrial mineral analogues. Interpretive errors may occur due to differences in the physical conditions of the cosmic and laboratory mineral dust grains. One of the potential artefact sources is that the wavelength and strength of resonances may be sometimes significantly influenced by the shape and size of the particles (Mutschke, Min & Tamanai 2009). Another important factor is the ambient temperature (Posch et al. 2007; Mutschke et al. 2008). While cosmic dust populations exist over a wide range of temperatures, from very cold to room temperature, most published laboratory spectra have been collected only at room temperature. Our investigations show significant temperature dependence for the absorption features, in agreement with the few previous mineral low-temperature far-IR spectral studies (Bowey et al. 2001, 2002; Chihara, Koike & Tsuchiyama 2001; Molster et al. 2002; Koike et al. 2006; Posch et al. 2007; Mutschke et al. 2008).

Variations in chemical composition even within the same mineral, and variations in crystallinity, are additional sources of interpretive ambiguity. Such variations are found within the same terrestrial mineral species of different provenance, due to differences in geologic histories, and similar variations might be expected for different dust populations in space. We demonstrate such spectral variations for a few sulphide minerals in this paper.

1.1 Astrophysical relevance of sulphide minerals

After H, He, C, N, O and Ne, the most abundant elements in the Galaxy and the Sun are those which the majority of astrophysical rocky materials are composed of, namely Si, Mg, Fe and S. Sulphur and sulphides are thus extremely common, found wherever solar abundance material is cooler than ∼800 K, the temperature at which gaseous sulphur condenses out of a vacuum. Keller et al. (2002) have discussed the condensation of solid metal sulphide species as a possible explanation of the deficit of atomic sulphur in dense cold molecular clouds surrounding YSOs, implying that iron sulphide might in fact be an important component of the circumstellar dust. Iron sulphides are also a predicted dust component in carbon-rich evolved stars. They are diagnostic of the local nebulae and cometary objects (Keller et al. 2002, 2006).

Pyrite, pyrrhotite, pentlandite and troilite are of potentially great astrophysical relevance. Two of these – pyrrhotite and pentlandite, in roughly 3:1 ratio – have been reported extensively in the *Stardust* sample return. Troilite has been reported in a few samples tested as well. Precise bulk abundances of species are inexact due to heating and alteration effects on the metal sulphides by the hot *Stardust* capture.

Many sulphide species, such as troilite (FeS), niningerite [(Mg,Fe)S], pentlandite [$(Fe,Ni)_9S_8$], and some hydrated sulphides, for example, from the tochilinite $\{Fe^{2+}_{5-6}(Mg, Fe^{2+})_5[(OH)_{10}|S_6]\}$ group, are found in meteorites (Rubin 1997). Iron sulphides, such as pyrrhotite [$(Fe_{1-x}S)$] and troilite, were found to be the two most common sulphides in anhydrous (cometary) interplanetary dust particles (IDPs), while hydrated IDPs contain more of the iron–nickel sulphides, such as pentlandite (Forrest et al. 1981; Tomeoka & Buseck 1984; Goebel & Moseley 1985; Rietmeijer 1989, 1993; Keller, Thomas & McKay 1993; Bradley 1994; Zolensky & Thomas 1995; Hony et al. 2002; Keller et al. 2002). Westphal et al. (2009) report abundant sulphides and a minimum S/Fe atomic ratio of 0.31 in cometary dust samples. A strong and broad emission feature in the IR spectra from C-rich evolved stars and planetary nebulae extending from 25 to 45 μm has been attributed to MgS, which has a strong absorption feature around 32–36 μm with shoulders at ∼22, 25 and 38 μm (Nuth et al. 1985; Kimura et al. 2005a).

1.2 Previous far-IR spectroscopic studies on sulphides

Relatively few far-IR spectral data exist in the literature on suitably characterized naturally occurring sulphide minerals to be useful for astronomical data analysis. However, some thorough studies on the IR properties of metal sulphides were performed a couple of decades ago, and these are summarized below to put our work in context and to present a unified body of work.

When the sulphides have low intrinsic conductivity, that is, have a large band gap and few free mobile electrons, the lattice vibrational modes dominate the absorption spectrum. More problematic cases occur with some sulphides, whose metallic conductivity (Nozaki, Shibata & Ohhashi 1991; Liang & Whangbo 1993) leads to broad IR absorption and a featureless spectrum, as, for example, in the case of pyrrhotite [$Fe_{(1-x)}S$] and covellite (CuS) (Soong & Farmer 1978). Far-IR spectra from 50 to 200 μm wavelength were discussed by Karr & Kovach (1969) for eight sulphides [including CaS, SrS, BaS, realgar (As_4S_4), orpiment (As_2S_3), stibnite (Sb_2S_3) and bismuthinite (Bi_2S_3)]. However, only for cinnabar (HgS) was the measured spectrum actually presented and none of these semimetal sulphides is likely to be astrophysically relevant. In Liese (1974), the peak frequencies and relative intensities are provided for 54 natural sulphides and sulphosalts, obtained using the KBr disc technique in the 23–40 μm wavelength range. Transmittance spectra in the 2.6–222 μm range for several sulphides (although in the form of chemical reagents) are given in Nyquist & Kagel (1971). In Gadsden (1975), IR peak frequencies and relative intensities are given for several of the sulphides (pyrite, marcasite, sphalerite/blende, galena) (see Table 1). A very informative study (Soong & Farmer 1978) presents spectra in the region 24–110 μm for 25 natural sulphides, including cinnabar, galena, pyrrhotite, alabandite, sphalerite, wurtzite, realgar, orpiment, stibnite, bismuthinite, arsenopyrite, tetrahedrite, pyrargyrite, proustite, enargite, bournonite, boulangerite, jamesonite and plagionite. The sulphide samples were finely ground and dispersed in polyethylene (PE) discs. Laboratory spectra and mass absorption coefficients of the synthetic chemical reagents MgS, CaS, FeS, SiS_2 and FeS_2, over the range 15–125 μm, are presented in Nuth et al. (1985). Lennie & Vaughan (1992) presented IR transmittance spectra in the range 16.7–33.3 μm for solid-state transformation of marcasite (FeS_2) into pyrite (FeS_2). Begemann et al. (1994) presented optical data for synthetic Mg–Fe sulphides with different Mg/Fe ratios in the 10–500 μm wavelength range, allowing a tentative attribution of the 30 μm emission band from circumstellar protoplanetary and planetary nebulae of carbon-rich stars to Mg-S vibrations in sulphides. Kimura et al. (2005a) discussed the considerable effect of grain shape and surface effects on the IR spectra of MgS. A possible contribution of Fe sulphides such as troilite (FeS), pyrrhotite ($Fe_{1-x}S$), pentlandite [$(Fe,Ni)_9S_8$] and pyrite (FeS_2) to

Table 1. Samples, their origin and AMNH mineral collection catalogue number, composition, crystal system, far-IR absorption peak position in μm, peak mass absorption coefficient κ_p (with reference to continuum baseline) and references to previously published far-IR sulphide studies (peak positions in μm and, where available, κ_p, in units of $cm^2\ mg^{-1}$). The estimated uncertainty in peak positions across the spectrum for well-defined bands is $<1\ cm^{-1}$, which is 1 μm at 100 μm wavelength and 0.5 μm at 50 μm wavelength, and so forth.

Mineral name	Sample origin, AMNH #	Actual sample composition	Crystal system	λ (μm)	Peak κ_p value ($cm^2\ mg^{-1}$)	Previously published far-IR data (μm)
$A_{2-x}X$						
Digenite	Silver Bow, MT, USA, 26782	$Cu_{8.84}Fe_{0.16}S_{4.95}$	Trigonal	Featureless	–	Featureless[d]
AX						
Galena	Rhodope Mountains, Bulgaria, 106792	PbS	Isometric	–	–	Featureless[d,e]
				59.2bM	0.73	60bS[a]
				–	–	27W[a]
				–	–	25W[a]
Alabandite	Allakhnyun, Russia, 103312	MnS	Isometric	–	–	Featureless[d]
				47.6bS	2.2	44bS[a]
				33.7M(sh)	0.83	33sh[a]
Sphalerite	(1) TN, USA, 109954 (2) Trepca, Yugoslavia, 25135	(1) $Zn_{0.92}Fe_{0.06}S$ (2) $Zn_{0.8}Fe_{0.2}S$	Isometric	32.3–32.9bS	1.8–3.0	32.7–35.7bS[a,d,e]
				30.2sh	1.3–1.5	30sh[a]
						24W[e]
						21.2W[e]
						18.8W[e]
Wurtzite	Pribram, Czechoslovakia, 26973	$Zn_{0.98}Fe_{0.02}S$	Hexagonal	34.5bS	3.1	33bS[a]
				30.1M(sh)	1.2	30sh[a]
Covellite	Bor, Serbia, 27339	CuS	Hexagonal	Featureless	–	Featureless[d]
Pyrrhotite	Chihuhua, Mexico, 52603	$Fe_{0.9}S$	Monoclinic	Featureless	–	Featureless [a,b,d]
						23bS[c]
AX_2						
Pyrite	(1) St. Agnes, England, 1717 (2) CO, USA, 37240	(1) FeS_2 (2) FeS_2	Isometric	34.1M	0.52–1.3	34–38M (0.2)[a,b,c,d]
				28.7S	1.4–2.3	28–29M (0.2)[a,b,c,d]
				25.1sh	0.93	24.3sh[e]
				24.2vS	2.6–5.1	24S (0.86)[a,b,c,d,e]
Marcasite	IL, USA, 38718	FeS_2	Orthorhombic	40vW	–	40W[a]
				34M	0.5	34W[a]
				30.5S	1.3	30M[a,d]
				28S	1.2	28M[a,d](sh)[e]
				25vS	2.7	25S[a,d]
				24vS	2.7	23.7–24S[a,d,e]
				23.1sh	1.5	23S[a]
				–	–	20.8sh[e]
Chalcopyrite	Ontario, Canada, 29392	$Cu_{1.02}Fe_{1.01}S_{1.97}$	Tetragonal	37.7W	0.22	38M[a]
				31S	1.2	32M[a,d]
				27.5S	2.1	28S[a,d]
				26.6S	1.7	27sh[a,d]
Stibnite type						
Stibnite	Romania, 110042	Sb_2S_3	Orthorhombic	208.3W(sh)	0.1	–
				172.4M	0.28	–
				147vW	0.03	–
				130W	0.12	–
				91M	0.37	100M[a]
				71S	1.1	70S[a]
				57.5S	1.05	59S[a]
				40.6S	1.4	40–41bS[a,d]
				35.2S	0.97	33–35vS(sh)[a,d]
				29.5S	0.59	30S[a,d]

Notes. S = strong; M = medium; W = weak; b = broad; sh = shoulder; v = very.
[a] Soong & Farmer (1978).
[b] Nuth et al. (1985).
[c] Hony et al. (2002).
[d] Liese (1974).
[e] Gadsden (1975).

an ∼23 μm feature of the carbon-rich evolved stars and planetary nebulae was discussed in Hony et al. (2002) and Keller et al. (2000, 2002). IR studies of sulphide minerals, but with no actual spectra presented, have been reviewed in Wincott & Vaughan (2006). In Pring et al. (2008), a systematic study of the sphalerite (Zn,Fe)S spectra for a range of Fe substitution is presented in the range 16.7–66.7 μm.

1.3 Objectives and scope

Objectives were to select and prepare powdered submicrometre-size sulphide mineral samples that represent the most abundant groups, to verify composition, homogeneity and structure, to measure the grain-size distribution, to prepare samples for far-IR spectroscopy, to collect their transmittance spectra, and to calculate and interpret mass absorption coefficients in the wavelength range 15–250 μm. The spectral range of *Herschel*'s Photodetector Array Camera and Spectrometer (PACS) instrument falls within this range. A novel feature compared to previous work is that Stokes settling is used to achieve a more uniform and narrow size distribution centred around ∼1 μm. This results in more accurate mass absorption coefficients than would be obtained if the samples included optically-thick particles. In addition, we present the effects of low temperature and provenance (on which the chemical composition and density of structural defects may depend) on the sulphide far-IR spectra.

Sulphide mineral species sampled in this work include digenite, galena, alabandite, sphalerite, wurtzite, covellite, pyrrhotite, pyrite, marcasite, chalcopyrite and stibnite. Pentlandite and troilite, two of the most astronomically relevant sulphides, were not available for sampling. Consequently, their spectra could not be included in this paper. Due to the necessity of publishing the other data in a timely fashion with respect to the ongoing *Herschel* mission, we reserve the spectroscopy of pendlandite, troilite and several other astrophysically-important sulphide minerals for a future supplemental publication.

The mineral selection was based on potential relevance to astronomical observations. Included are minerals identified in meteorites, in the *Stardust* return, and (tentatively) in the planetary nebulae, supernova remnants or circumstellar discs. In some cases, minerals containing relatively rare elements (e.g. Sb, Zn, Pb, Mn) were selected as well, because these have very distinct far-IR bands, whose strength potentially might compensate (i.e. in astronomical spectra) for their relatively low cosmic abundance.

All spectra are presented with a linear wavenumber scale, because linewidths then tend to be similar throughout the spectral range. On a linear wavelength scale, linewidths increase rapidly with increasing wavelength, causing weaker features at the longest wavelengths to become invisible in the plot. Wavelength ticks are provided on the top axis of each plot, though this scale is non-linear. All data files will be made available online via the planetary data system.

2 EXPERIMENTAL METHODS

2.1 Mineral selection and initial characterization

Mineral grains and fragments were selected from the American Museum of Natural History (AMNH) mineral collection and crushed to separate intergrowths as appropriate. Clean grains were hand selected under a stereo microscope and crystallographically verified via X-ray multigrain microdiffraction (Rigaku DMAX/Rapid) and powder diffraction (Philips 1710 Bragg-Brentano) diffractometers. Electron microprobe analysis (Cameca SX100) of polished grains verified chemical composition, stoichiometry, and micrometre-scale homogeneity.

2.2 IR sample preparation

Mineral samples were ground to powders of average particle size <10 μm to minimize scattering (Coleman 1993), whose signature is a decreasing transmittance baseline with decreasing wavelength. A McCrone Micronizing Mill was used to reduce particles up to 0.5 mm dimension to micron sizes using cylindrical grinding elements that produce both line contact blows and planar shearing, in contrast to the random contact blows of a conventional ball mill. Slurry grinding in cyclohexane or mineral spirits, with either corundum or agate grinding elements, was used for mineral samples to minimize defect introduction into the crystalline particulates (Bish & Reynolds 1989). Oxidation of powders is a particular difficulty as the surface area of metal sulphide grains is increased during comminution. Mineral spirits were found optimal for avoiding potential oxidation of Fe sulphides.

After grinding, the small-size fraction was separated by Stokes settling. Here the ground mineral powders were suspended in acetone, and the fraction that remained suspended after a certain time τ was collected and dried at room temperature overnight, as described in Mutschke et al. (2008). The sedimentation time τ, assuming spherical particles of ∼5 μm radius, was obtained from Stokes' formula $\tau = 9\mu h/2gR^2(\rho_p - \rho_f)$, where g is the gravitational acceleration, ρ_p is the mass density of the mineral, ρ_f is the mass density of acetone, R is the spherical particle radius, μ the fluid's dynamic viscosity, and h is the settling height. Particle size distribution histograms were determined from scanning electron microscope (SEM) images (Fig. 1) to confirm the expected size distributions resulting from Stokes settling. Here, the average dimension of 100–400 particles with clearly defined borders was determined from two to four SEM images.

A fine distribution of mineral grains in PE was achieved by thoroughly mixing the desired mineral mass with incremental additions of ∼700 mg of PE powder (Mitsui Chem MIPELON XM-220 PE microparticles, 30 μm average size). To avoid saturation of the absorption features in transmittance, the total effective thickness of mineral in each PE sample must be no more than several μm (which necessitates the fine particle size distribution). This condition is satisfied by mineral content of ∼4–6 mg per pellet (∼0.6–0.9 wt per cent) (Brügel 1962; Coleman 1993). The mixture was transferred to a home-made teflon pelletizer, where plunger rotation levels the

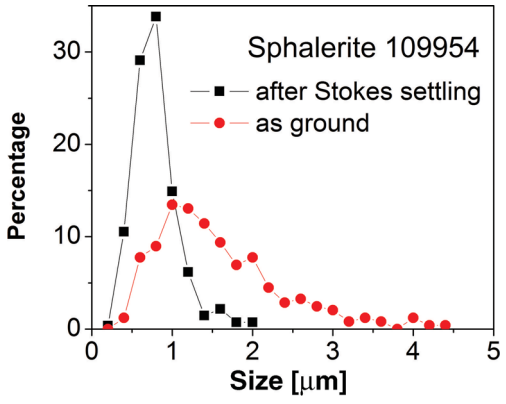

Figure 1. Examples of sulphide powder size distributions, as ground, and the fine fraction powder collected after Stokes precipitation.

sample. Hot pressing at controlled temperature (<130°C) for ∼30 min transforms the powder to a uniform translucent pellet of 2.9 cm diameter and ∼1 mm thickness (Brusentsova et al. 2010, 2011).

2.3 Far-IR spectroscopy

A Bomem DA8 vacuum-bench Fourier spectrometer was used to collect transmittance spectra. Resources used were a globar source, 12- and 3-μm Mylar pellicle beamsplitters, and a 4 K Si bolometer. The useable spectral range was 40–650 cm^{-1} (250–15.4 μm wavelength). A spectral resolution of 4 cm^{-1} was found adequate to resolve all far-IR mineral features, except in pyrite where 2 cm^{-1} resolution was required to resolve some of the bands. Two pellets were measured, one with and one without mineral. The transmittance T was calculated as the ratio of the transmitted power spectra for the two. The wavenumber accuracy of the spectrometer is specified as $\pm 0.001\ \mathrm{cm}^{-1}$. The uncertainty in determining the centre frequencies for well-defined bands throughout the spectrum was less than 1 cm^{-1}. This corresponds to 1 μm at 100 μm wavelength and 0.5 μm at 50 μm wavelength, and so forth. The uncertainty in the baseline is ∼5 per cent, which appears sometimes as a mismatch of the baselines where the spectral range of different beamsplitters overlaps.

Low-temperature measurements were obtained by cooling the pellets down to ∼16 K in a closed cycle refrigerator. The tailstock of the cryostat cold head was inserted into the spectrometer vacuum sample compartment via an o-ring muff-coupler. The windows on the tailstock were PE. A 1-kΩ carbon resistor embedded with Apiezon N-grease in the copper cold finger was used to monitor the temperature. The pellet under test was attached to the cold finger with rubber cement.

The absorbance $\alpha d = -\ln(T)$ calculated from the measured transmittance T is proportional to the effective mineral thicknesses d, which is the thickness of the imaginary film that would be formed if all the suspended mineral powder were to condense into a uniform continuous layer with the same cross-sectional area S as the pellet. The absorption coefficient is α in units of cm^{-1}. Values for d of just a few μm are necessary to avoid saturating the measured transmittance T. The effective thickness d is $m/(S\rho)$, where m is the mass of mineral in the pellet and ρ is the mineral density. Accurate determination of absorption coefficients from the measured T requires uniform mineral thickness across the beam diameter, which means that the particle sizes must be less than d. The *mass* absorption coefficient $\kappa = \alpha/\rho$ in $\mathrm{cm}^2\ \mathrm{g}^{-1}$ is the absorption cross-section per 'molecule' divided by the mass per 'molecule'. More directly $\kappa = (S/m)\ln(1/T)$.

To determine the quantitative accuracy and repeatability of the mass absorption coefficients obtained by our technique, pellets with different loadings of spinel ferrite and of phyllosilicate montmorillonite were measured with absorbance values up to 4.5. The absorbance values varied monotonically with concentration, with scatter amounting to less than 10 per cent. The deviation from linear dependence on concentration at absorbance values of up to 3 (transmittance = 5 per cent) was less than 20 per cent, with a systematic tendency to overestimate mass absorption by this amount at the highest absorbance values. In other words, for typical pellet loading of 4 mg, determined mass absorption coefficient values as high as ∼5 $\mathrm{cm}^2\ \mathrm{mg}^{-1}$ are possibly overestimated by up to 20 per cent. The bolometer itself is considered to have a linear response, so that any systematic non-linear concentration effect is attributable to some property of the sample itself. However, none of the spectra presented here approaches such high values of mass absorption coefficient. Consequently, we assert that the uncertainty for κ values presented in this paper is less than 10 per cent.

The thermal emission intensity $\mathrm{d}I$ in the frequency range $\mathrm{d}\omega$ per unit mass of dust is found according to $\mathrm{d}I = 4\pi\, c\kappa(\omega)\ \mathrm{e}_0(\omega)\,\mathrm{d}\omega$, where $\mathrm{e}_0(\omega)$ is the Planck blackbody function. This formula is an approximation that holds for an isothermal dust cloud in the limit that the absorptance $A = 1 - T$ (neglecting reflectance) never approaches unity at any wavelength, which holds for particle sizes less than a few μm. Optically-thick dust populations, which have nearly unity absorptance at all wavelengths, likewise have spectrally uniform emissivity if they are isothermal. In such a case, the characteristic mineral features contained in $\kappa(\omega)$ would be absent from the emission spectrum. If temperature gradients occur, characteristic features can appear in either absorption or emission.

3 RESULTS

3.1 IR features

Minerals sampled are summarized in Table 1. Of all the sulphides studied, only stibnite and galena have definite and significant features within the PACS range (57–210 μm), although chalcopyrite tentatively has a weak band at 112 μm wavelength. The positions and intensity of the peaks for both agree well with those in Soong & Farmer (1978). The characteristic features of the other sulphides fall at shorter wavelengths. Overall, the comparison of the currently presented spectra with available published data shows good agreement, with some minor discrepancies.

Fig. 2 presents mass absorption coefficient spectra for the AX_2-type sulphides: pyrite (FeS_2), marcasite (FeS_2) and chalcopyrite ($CuFeS_2$). The two Fe-sulphide polymorphs have similar spectra, except that marcasite has additional lines because its orthorhombic

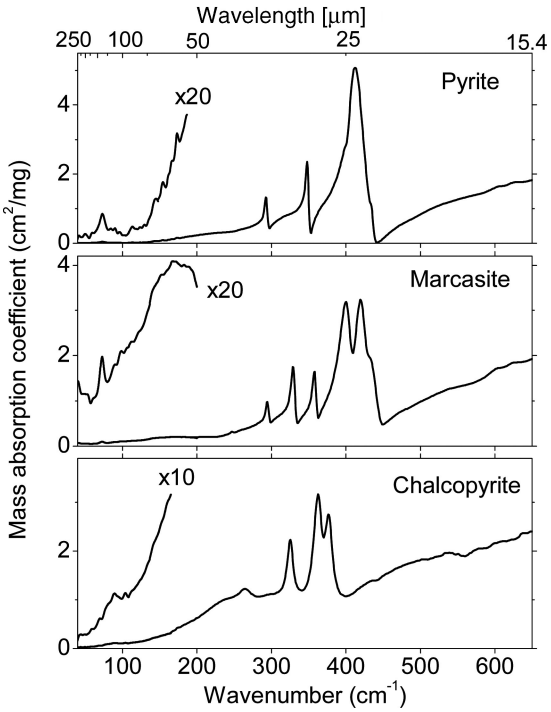

Figure 2. Mass absorption coefficient spectra at room temperature for AX_2-type sulphides [pyrite (FeS_2), marcasite (FeS_2), chalcopyrite ($Cu_{1.02}Fe_{1.01}S_{1.97}$)]. The uncertainty in absorption values is less than 10 per cent.

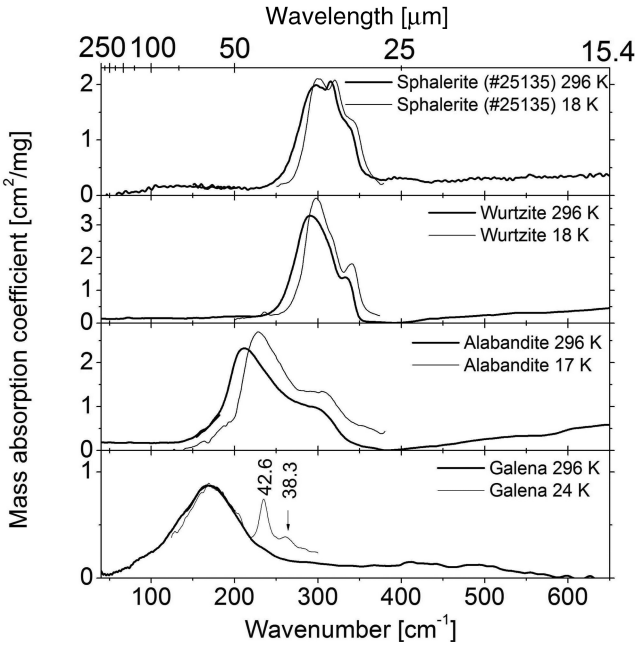

Figure 3. Mass absorption coefficient spectra for AX-type sulphides [wurtzite ($Zn_{0.98}Fe_{0.02}S$), sphalerite ($Zn_{0.8}Fe_{0.2}S$), alabandite (MnS) and galena (PbS)], at room and low temperatures. The labelled peaks in the low-temperature galena spectrum are artefacts. The uncertainty in absorption values is less than 10 per cent. The peak labels are centre wavelengths in μm.

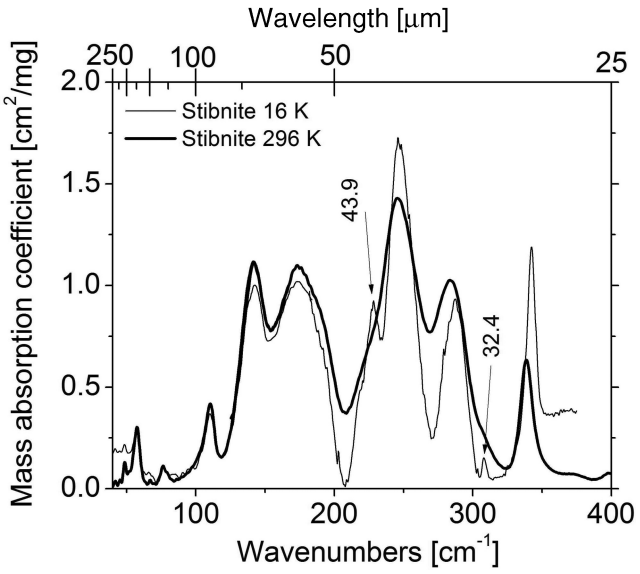

Figure 4. Mass absorption coefficient spectra for stibnite (Sb_2S_3), at room and low temperatures. The uncertainty in absorption values is less than 10 per cent. The peak labels are centre wavelengths in μm.

symmetry is lower than that of cubic pyrite. A particular difference of note is the splitting in marcasite of the strong band in pyrite near 25 μm. When half the Fe ions are replaced with the heavier Cu to form tetragonal chalcopyrite, the spectrum redshifts by about 3.1 μm. The lines, especially in the iron sulphides, have a characteristic asymmetry, being sharper on their shorter wavelength sides.

A weak feature at 73 cm^{-1} for pyrite and marcasite should be considered with caution. PE has an absorption here, so that small differences in the thicknesses of the sample and reference pellets may result in an artefact at these wavenumbers. A weak band at 89.4 cm^{-1} for chalcopyrite is sufficiently removed that it may be considered as real, though is so weak that we do not include it in Table 1.

Liese (1974) found that for chalcopyrite an increase in Cu content redshifts the 27-μm band but *blueshifts* the 27.8-μm band. Soong & Farmer (1978) reported for chalcopyrite a medium peak at 37.9 μm, a strong peak at 31 μm and a strong doublet at 27.7 and 26.7 μm, while for pyrite two medium peaks at 34 and 28.6 μm, and a strong peak with a shoulder at 24–25 μm were found. Additionally, for marcasite were found weak peaks at 40.5 and 33.8 μm, medium peaks at 30.4 and 28.1 μm, and a strong triplet with peaks at 24.8, 23.6 and 22.9 μm. Nuth et al. (1985) reported two sharp peaks at 38 and 29 μm in pyrite and a stronger and broader feature centred at 24 μm. Hony et al. (2002) reported for pyrite a dominant line at 24 μm and two weaker but sharp peaks at 28.5 and 34 μm. All the above-mentioned peak positions and relative intensities from the reference studies corroborate well with our data (see Table 1).

Fig. 3 presents spectra for AX-type sulphides [wurtzite (ZnS), sphalerite [(Zn,Fe)S], alabandite (MnS) and galena (PbS)]. The single bands in wurtzite and sphalerite, which are both predominantly Zn sulphides, occur at similar positions. Overall, a remarkable redshift of the characteristic absorption band in the sequence of cubic sphalerite → alabandite → galena (32.3 → 47.6 → 59.2 μm peaks, respectively) is correlated with an increase in the atomic radii of the metal cation in this series. For six-fold coordinated, divalent ions in oxide crystals, we have for the sequence of radii (in Å) Zn(0.75) < Mn(0.67, 0.83) < Pb(1.18) (see table 2.1 of Kaminskii 1990).

Liese (1974) reported no absorption features for galena, while for sphalerite an increase in Zn content was correlated with a redshift. In contrast, Soong & Farmer (1978) found that galena exhibits a strong broad absorption band centred at 60.2 μm and two very weak features at 26.8 and 25.1 μm, while wurtzite, sphalerite and alabandite spectra show remarkable redshift of the main absorption band for all three cases (see Table 1 for details) that correlates with increasing average cation radius in the series Zn → Fe → Mn.

Fig. 4 presents a spectrum of the X_2S_3 sulphide stibnite (Sb_2S_3). This mineral has a rich spectrum, including prominent peaks in the range of PACS. The Karr & Kovach (1969) absorption frequencies and relative intensities for stibnite (42S, 37shS, 30M) corroborate well with our data. Liese (1974) found for stibnite that an increase in Sb content causes a blueshift to shorter wavelengths in at least one of the major absorption bands (from 30.1 to 29.8 μm). Soong & Farmer's (1978) stibnite spectrum shows a broad structured band with features at 100, 69.9, 58.8, 41, 35.3 and 29.8 μm. Several absorption features beyond 100 μm, which were not previously reported (to the best of our knowledge), are resolved in our spectrum (Table 1 and Fig. 4).

It was realized by Soong & Farmer (1978) and Liese (1974) that the conductivity of some of the metallic sulphides, for example, troilite, covellite, pyrrhotite (Nozaki et al. 1991; Liang & Whangbo 1993), leads to broad absorption in the IR and nearly featureless transmittance spectra, with absorption increasing monotonically towards shorter wavelengths. Nuth et al. (1985) reported that pyrrhotite ($Fe_{1-x}S$) possesses such a smoothly sloping spectrum for wavelengths below 125 μm. Fig. 5 presents examples of such relatively featureless spectra for covellite (CuS), pyrrhotite ($Fe_{0.9}S$) and digenite ($Cu_{8.84}Fe_{0.16}S_{4.95}$).

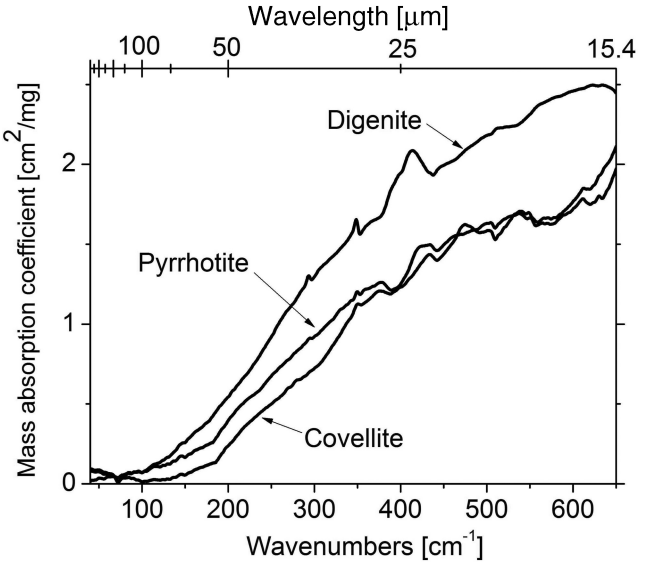

Figure 5. Examples of nearly featureless absorption spectra for sulphides with metallic conductivity [covellite (CuS), pyrrhotite ($Fe_{0.9}S$), digenite ($Cu_{8.84}Fe_{0.16}S_{4.95}$)].

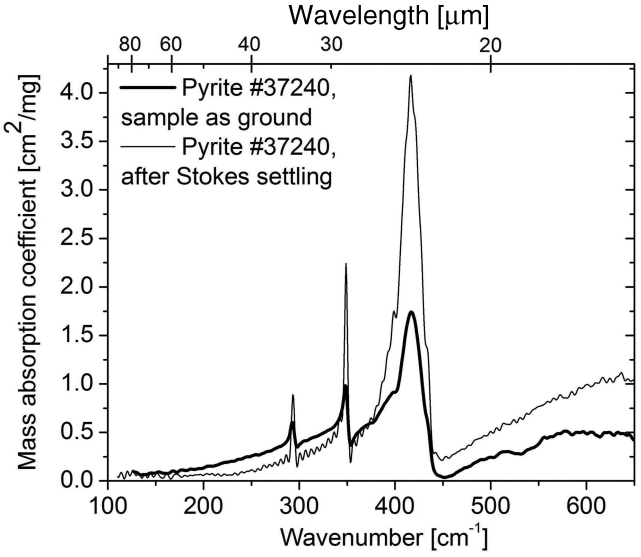

Figure 6. Example of the particle size distribution effect on the pyrite spectrum. IR samples were prepared with the same pyrite (#37240) powder 'as ground' and with the fine fraction powder collected after Stokes precipitation. The uncertainty in absorption values is less than 10 per cent.

3.2 Factors influencing IR-band position and intensity

3.2.1 Particle size effect

The accuracy of the mass absorption coefficient spectra is substantially affected by the particle size distribution within the sample. Fig. 1 presents the particle size distributions for the mineral sphalerite before and after Stokes precipitation, which was designed to produce a distribution with particle sizes less than 5 μm. In the original size distribution, all the particles were already smaller than this, with a peak in the distribution at 1 μm. However, for the 4.5-μm particles near the tail of the distribution, using a peak mass absorption coefficient of 2 cm^2 mg^{-1} from Fig. 3 and the ∼4 g cm^{-3} density of sphalerite, the transmittance would be less than 3 per cent. Thus, a pellet made with the original size distribution would have a rather non-uniform transmittance over the pellet cross-section, with the larger components acting like 'Venetian blinds'. Then the actual mass of mineral in the pellet that is interrogated in the transmittance measurement would be less than the total mass m that was added to the pellet and used in calculating the mass absorption coefficient, resulting in an underestimate of the latter.

After Stokes precipitation, the bulk of the sphalerite particles are below 1.5 μm with a peak in the distribution less than 1 μm. Fig. 6 shows how Stokes settling leads to higher (and more accurate) mass absorption coefficient values. The spectra for pyrite before and after Stokes precipitation are presented. After Stokes precipitation, we notice the intensities of the absorption lines all increase by factors of about 3. Additionally, the lines have become sharper. The ringing in the wings of two of the lines in the Stokes settled sample is an artefact of boxcar apodization for lines that have become narrower than the 4 cm^{-1} instrumental resolution chosen for these measurements. Such a substantial difference between the spectra taken for the powdered pyrite sample before and after Stokes settling demonstrates the importance of such pretreatment to eliminate the optically-thick size fraction and to allow an effective mineral thickness that is uniform across the pellet.

Another possible size- and shape-related artefact is a shifting of the peak frequencies. The influence of grain shape and surface on IR spectral features of MgS has been discussed in Kimura et al. (2005a). The main far-IR absorption peak for cubic MgS grains at ∼32 μm was reported to shift to ∼40 μm for spherical or network-like shaped grains. We do not observe significant changes in peak positions after our Stokes settling procedure, which rules out any significant size effect of this nature. As we have no control over particle shape distributions, shape effects remain a question.

3.2.2 Provenance effect

Liese (1974) reported significant dependence of peak intensities and frequencies on mineral provenance. These effects can originate from variations in chemical composition and/or crystallographic defect density, due to environmental effects during the formation of the minerals. The dependence of the shape of the absorption features on variations in chemical composition has been systematically studied in Pring et al. (2008) for sphalerite [(Zn,Fe)S], where the main absorption line splits as the FeS content in ZnS increases from 0 up to 24 mol per cent. The initial single peak at 31.2 μm for 0 per cent FeS transforms into a doublet with maxima at 31.7 and 33.3 μm, where 31.7 μm is due to the main ZnS structure, and the 33.3-μm peak is attributed to FeS impurity.

Fig. 7 demonstrates the variability of the far-IR absorption spectra for mineral samples of different provenance for sphalerite (see also Table 1). The two sphalerites demonstrate an increase in the main line splitting with increasing FeS content, as reported by Pring et al. (2008) (see also Table 1). In addition, there is a change in the relative strength of the two components.

3.2.3 Low-temperature effect

The importance of temperature on mineral spectra has been pointed out in several studies (Bowey et al. 2001, 2002; Chihara et al. 2001; Molster et al. 2002; Koike et al. 2006; Posch et al. 2007; Mutschke et al. 2008). The shape and strength of spectral features of many materials is temperature sensitive (Waters 2009). Cooling tends to shift line-centre frequencies towards shorter wavelengths, which is attributed to lattice contraction. Lines tend also to sharpen and

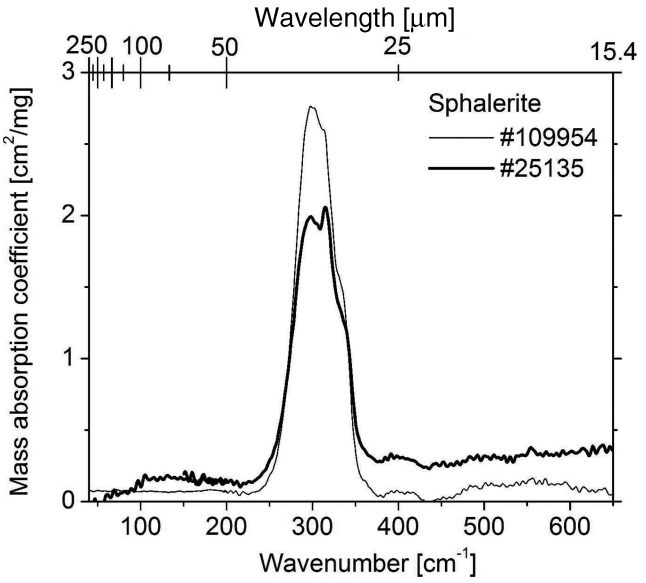

Figure 7. Example of provenance effect on the IR spectra of sphalerite [#109954 ($Zn_{0.92}Fe_{0.06}S$), #25135 ($Zn_{0.8}Fe_{0.2}S$)]. The uncertainty in absorption values is less than 10 per cent.

deepen due to decrease in phonon density at lower temperatures. Such blueshifting and sharpening of the bands with decreasing temperature have been reported in forsterite (e.g. Koike et al. 2006). More striking is that splitting (or more accurately, the resolution of overlapping bands) occurs at low T, new features appear, and the relative strengths of different lines in the spectrum may change. These effects are particularly important, considering that cold dust formations are among the main targets of observations by the remote IR missions such as *Herschel*. Figs 3, 4 and 8 show such low-temperature effects on the IR spectra.

Fig. 3 presents the temperature dependence of the AX-sulphide spectra. Cooling causes a remarkable blueshift of the main broad absorption band for sphalerite, wurtzite and alabandite. The low-temperature spectrum of galena contains two artefact peaks at 42.6 and 38.3 μm due to a thin layer of ice that is cryopumped on to the pellet. This non-repeatable effect presumably occurs when the vacuum jacket of the cryostat is not pumped down enough, or perhaps due to leaking seals. It was confirmed by collecting a low-temperature spectrum of the reference pellet with an intentionally poor cryostat vacuum. This spectrum is presented 'as is' to serve as a caution regarding the appearance of these lines in laboratory low-temperature spectra. The line at 42.6 μm has been identified by others as due to water ice (Moore & Hudson 1992, 1994; Maldoni et al. 1999). The line at ∼38 μm is of uncertain attribution though definitely also correlated with poor cryostat vacuum.

The low-temperature spectrum of stibnite (Fig. 4) shows an overall sharpening of the absorption features and a blueshift for two of the major peaks. In addition, there is one additional weak absorption peak resolved at 32.4 μm, which appears as just a shoulder on the room-temperature spectrum. Also, a peak shows up at 43.9 μm, which nearly coincides with an ice line. However, the room-temperature spectrum has an unusual line shape at that position, which could be interpreted as an unresolved shoulder that emerges as a separate feature at low temperature.

The low-temperature chalcopyrite spectrum (Fig. 8) contains the two ice artefacts. Similarly, the low-temperature pyrite (#1717) spectrum (Fig. 8) also has the water ice peak at 42.6 μm, though the

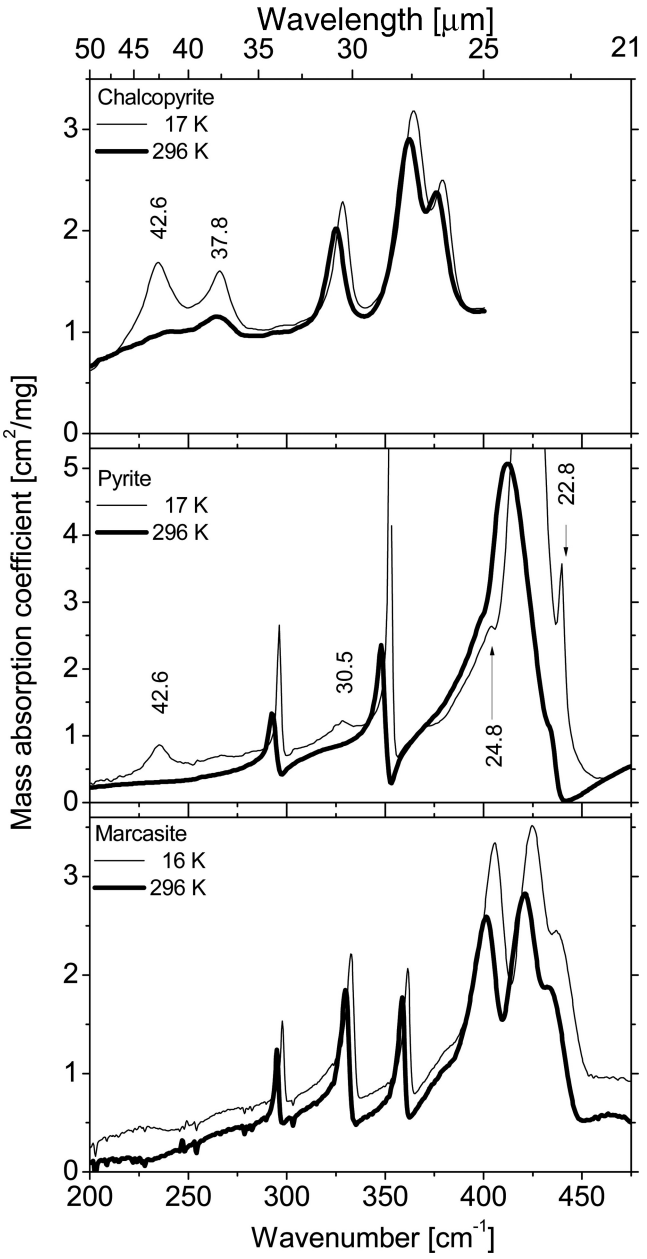

Figure 8. Effect of low temperature on far-IR spectra of chalcopyrite, pyrite and marcasite. The uncertainty in absorption values is less than 10 per cent, except for the saturated peaks in the low-temperature spectrum of pyrite. The peak labels are wavelengths in μm.

∼38 μm artefact is relatively weak. Additionally, possibly pyrite-attributed features at 24.8 and 22.8 μm appear, which are just shoulders in the room-temperature spectrum. The new feature at 30.5 μm at low temperature is of uncertain origin. (The two strongest lines in the pyrite spectrum were saturated in the low-temperature transmittance spectrum, so that these lines are truncated in the Fig. 8 absorption spectrum.) The blueshifts on cooling observed in these spectra are 2–4 cm^{-1}. Ice artefacts are absent in the spectrum of marcasite.

4 DISCUSSION

As an example application of the results presented here, our spectra may help to improve the analysis of material excavated from Comet

9P/Tempel 1 by the *Deep Impact* (*DI*) experiment. On 2005 July 4, the *Spitzer* imaging spectrometer was used to observe Comet 9P/Tempel 1 during the *DI* encounter (Lisse et al. 2006). The material that was ejected by *DI* was pristine and unaltered, due to the weakness of the cometary material and the low escape velocity (1 m s^{-1}) from the cometary surface. At the same time, it was de-aggregated from loosely held fractal particles into its individual subfractal components (A'Hearn et al. 2005; Sunshine et al. 2006). This resulted in a near-perfect IR spectroscopy experiment, giving detailed, highly structured 5–35 μm emission spectra of the ejecta, with over 16 sharp diagnostic spectral features, at a flux level ∼ 1 Jy. The material was all at 1.51 au from the Sun when observed, had cooled from any effects due to the impact within minutes, and the separation from the ambient coma dust was cleanly made. Characteristic emission signatures due to abundant rock-forming silicate, phyllosilicate (e.g. clays), and metal sulphide (e.g. pyrite) species, organic amorphous carbon, carbonate (chalk) and polycyclic aromatic hydrocarbon species, and water ice and gas were found. The ejecta spectra and the material emitted are very similar to those from Comet C/1995 O1 (Hale-Bopp), the circumstellar material around the YSO HD 100546 (Lisse et al. 2007), and the materials found in the in situ fly-by through the coma of Comet 1P/Halley. *DI* confirmed evidence for very Fe rich olivines, Ca/Al/Mg pyroxenes, and Mg and Fe carbonates also reported in the *Stardust* sample return for Comet 85P/Wild 2. *Stardust* samples have also proved to be much more processed, both mineralogically and isotopically, than a simple pristine collection of pre-solar nebula material would be – in fact, they look to be more solar like than the most primitive meteorites collected on the Earth, believed to be derived from infallen pieces of processed asteroidal material formed within the a few au of the Sun. The high crystallinity of the *Stardust* samples (modulo the masking of amorphous silicate materials by capture into amorphous silica aerogel) and solar isotopic abundances support the *DI* finding that the early solar nebula was the scene of high radial mixing – amorphous interstellar medium (ISM) silicates would only anneal inside the orbit of Mercury, while comets were formed at 5–50 au.

There is, however, currently some disconnect between the *Stardust* and *DI* results. First, the nature of the (Fe, Al, Na) phyllosilicates (clays) reported in Lisse et al. (2006) is uncertain. Secondly, the Fe/Mg sulphides used as *DI* models were instead found in the *Stardust* sample return to be Fe/Ni sulphides, like pyrrhotite and pentlandite (Zolensky et al. 2006). The differences between the two sets of results may be explainable by impact processing or the action of warm liquid, associated with the *Stardust* sample collection, when the capturing of the cometary particles (which initially could have contained water ice) into amorphous silica aerogel at ∼6.8 km s^{-1} velocity was accompanied by heating to ∼500–2000 K. The latter effect may be responsible for the difference between the laboratory analysis of the returned particles and the remote *Spitzer* spectra from *DI*. Also, mobile water may have affected Tempel 1 material. Such water may have been released during the formation of the two impact craters straddling the *DI* excavation site, or water may have been released during the over 40 close solar perihelion passages that eroded and altered the heavily processed Tempel 1 surface.

Before the *DI* and *Stardust* missions, many researchers viewed comets as mostly pristine collections of ISM material that were much too cold to change, even though there were strong indications of abundant crystalline silicates in the bright and active Comet Halley (e.g. Campins & Ryan 1989) and comet Hale-Bopp (e.g. Crovisier et al. 2000), very unlike the amorphous silicates observed in the ISM (Kemper, Vriend & Tielens 2004). However, now even the *Stardust* samples seem altered down to the isotopic level (Brownlee et al. 2006), appear to be mixtures of solar abundance materials (Lisse et al. 2007), and even have petrological characteristics similar to heavily processed asteroidal IDP material (Ishii et al. 2008). New work by Nesvorny et al. (2010) also suggests that highly processed IDPs previously thought to be differentiated asteroidal materials are of cometary origin. Parent-body alteration may also explain the apparent lack of abundant troilite in cometary dust, the expected kinetic product.

Alternatively, the differences could have been due to poor laboratory models for the dust species present. For instance, Fe and Fe–Ni sulphides such as pyrrhotite ($Fe_{1-x}S$), troilite (FeS) and pentlandite [$(Fe, Ni)_9S_8$] have been considered as potential candidates to explain the '23.5–24.5 μm' feature in the *ISO* spectra of YSOs and comet Hale-Bopp (Keller et al. 2000, 2002; Hony et al. 2002). Knowledge of the IR emission spectra of metal sulphides in 2006 was scanty. The best available models were the thin microtome slab measurements of Keller et al. (2002) on pyrite, pyrrhotite and troilite, covering a small wavelength range. Such attribution of the '23.5–24.5 μm' feature was based on IR spectra of ultramicrotome ∼70 nm thick sections of both terrestrial sulphides and extraterrestrial pyrrhotite grains extracted from primitive meteorites and chondritic anhydrous IDPs (Keller et al 2000). These measurements revealed strong sharp peaks for both pentlandite and pyrrhotite at ∼24.5 μm, in addition to broad asymmetric absorption centred at 23.5 μm. Next, Keller et al. (2002) performed similar measurements on thin pyrrhotite sections which showed a strong broad absorption feature centred at ∼23.5 μm, as found also in pyrrhotite-rich IDPs. As a result of a comparison of these laboratory spectra with the ISO spectra, it was concluded that the 23.5–24.5 μm band in *ISO* spectra of YSOs should be attributed to nanometre-size pyrrhotite grains, which supposes pyrrhotite to be a common component of circumstellar dust. These laboratory spectra disagree with other studies, including this work, which find no characteristic far-IR features for fine pyrrhotite particles embedded in KBr or PE (e.g. Liese 1974; Soong & Farmer 1978; Nuth et al. 1985). Similarly, Kimura et al. (2005b) found, for pyrrhotite <100 nm particles embedded in PE, mainly a monotonically sloping absorption in the 15.4–200 μm range with some weakly pronounced structure on top of the main baseline. The pyrrhotite spectrum presented here (Fig. 5) for particles of average size < 1 μm is also represented by a nearly featureless sloping baseline. Such discrepancies are intriguing, and so far may be explained only by a difference of the spectroscopic or sample preparation techniques. Deviations of the synthetic spectra from the observations are possibly related to grain shape effects and uncertainties in the iron content of the dust grains. The appearance of 23.5–24.5 μm absorption features in specimens with sub-100 nm dimensions may be a size effect, in which case the sulphide grains within space dust formations must have similar dimensions if the previous interpretation of the 23.5–24.5 μm features in the *ISO* spectra is correct. Also, disagreement between the models based on laboratory spectra and actual *ISO* spectra arises. For example, Hony et al. (2002) noted that the 23.5–24.5 μm band strength for astronomical and laboratory spectra corresponds poorly, and that this cannot be explained as a temperature effect. Additionally, the presence of resonances attributable to FeS in the observed spectra of protoplanetary discs has recently been questioned by Juhász et al. (2010). The analysis of a large set of spectra of protoplanetary discs taken with the *Spitzer*/IRS provided no evidence for FeS, contrary to studies based on older *ISO* spectra. Hence, although iron sulphides like pyrrhotite, troilite and pentlandite are abundant in meteorites and IDPs, and may be similarly abundant within the space dust

formations, attribution of the 23–24 μm *ISO* band to these sulphides is uncertain. The question remains as to which spectra best represent the cosmic dust conditions, the one with submicrometre sulphide particles equally distributed in IR transparent matrix, or the one measured on the ultramicrotome thin sections. New and better laboratory sulphide spectra may help to explain the three poorly fit features at ∼22, 24 and 29 μm in the 4 July 2005 5–35 μm *Spitzer*/IRS spectrum of the *DI* ejecta (Lisse et al. 2006).

5 SUMMARY

The far-IR mass absorption coefficient spectra of several groups of natural sulphide minerals have been presented and discussed. Comparison was made to previous studies, and some of the important sulphide-related astrophysical questions were discussed. The effects of particle size distribution, provenance and temperature were considered. The observed effects of low temperature on the IR spectra demonstrate the importance of having such low-temperature spectral data for all the cosmic matter relevant minerals in order to provide a basis for an adequate comparison of laboratory and astronomical peak wavelengths and intensities.

ACKNOWLEDGMENT

This research was supported by NASA-JPL Contract # 1327221.

REFERENCES

A'Hearn M. F. et al., 2005, Sci, 310, 258
Begemann B., Dorschner J., Henning T., Mutschke H., Thamm E., 1994, ApJ, 423, L71
Bish D. L., Reynolds R. C., Jr, 1989, in Bish D. L., Post J. E., eds, Modern powder diffraction. Min. Soc. Am., Washington, DC, p. 73
Bowey J. E., Lee C., Tucker C., Hofmeister A. M., Ade P. A. R., Barlow M. J., 2001, MNRAS, 325, 886
Bowey J. E. et al., 2002, MNRAS, 331, L1
Bradley J. P., 1994, Geochim. Cosmochim. Acta, 58, 2123
Brownlee D. et al., 2006, Sci, 314, 1711
Brügel W., 1962, An Introduction to Infrared Spectroscopy. Methuen, London
Brusentsova T. N., Peale R. E., Maukonen D., Harlow G. E., Boesenberg J. S., Ebel D., 2010, Am. Mineral., 95, 1515
Brusentsova T., Peale R. E., Maukonen D., Figueiredo P., Harlow G. E., Ebel D., 2011, Proc. Lunar Planet. Sci. Conf. XXXXII, p. 1457
Buss R. H., Tielens A. G. G. M., Cohen M., Werner M. W., Bregman J. D., Witteborn F. C., 1993, ApJ, 415, 250
Campins H., Ryan E. V., 1989, ApJ, 341, 1059
Carpenter J. M. et al., 2009, ApJS, 181, 197
Chen C. H. et al., 2006, ApJS, 166, 351
Chiavassa A., Ceccarelli C., Tielens A. G. G. M., Caux E., Maret S., 2005, A&A, 432, 547
Chihara H., Koike C., Tsuchiyama A., 2001, PASJ, 53, 243
Cohen M., Barlow M. J., Sylvester R. J., Liu X.-W., Cox P., Lim T., Schmitt B., Speck A. K., 1999, ApJ, 513, L135
Coleman P. B., 1993, Practical Sampling Techniques for Infrared Analysis. CRC Press, Boca Raton, FL
Crovisier J. et al., 2000, in Sitko M. K., Sprague A. L., Lynch D. K., eds, ASP Conf. Ser. Vol. 196, Thermal Emission Spectroscopy and Analysis of Dust, Discs and Regoliths. Astron. Soc. Pac., San Francisco, p. 109
Farmer V. C., 1974, Infrared Spectra of Minerals in Mineralogical Society Monograph 4. Mineralogical Society, London
Forrest W. J., Houck J. R., McCarthy J. F., 1981, ApJ, 248, 195
Gadsden J. A., 1975, Infrared Spectra of Minerals and Related Compounds. Butterworths, USA
Gehrz R. D., Becklin E. E., de Pater I., Lester D. F., Roellig T. L., Woodward C. E., 2009, Adv. Space Res., 44, 413
Glaccum W., 1995, in Haas M. R., Davidson J. A., Erickson E. F., eds, ASP Conf. Ser. Vol. 73, Airborne Astronomy Symposium on the Galactic Ecosystem: From Gas to Stars to Dust. Astron. Soc. Pac., San Francisco, p. 395
Goebel J. H., Moseley S. H., 1985, ApJ, 290, L35
Hanner M. S., 1985, Adv. Space Res., 5, 325
Harvey P. M., Thronson H. A., Gatley I., 1979, ApJ, 231, 115
Henning Th., 2010, ARA&A, 48, 21
Hony S., Bouwman J., Keller L. P., Waters L. B. F. M., 2002, A&A, 393, L103
Ishii H. A., Bradley J. P., Dai Z. R., Chi M., Kearsley A. T., Burchell M. J., Browning N. D., Molster F., 2008, Sci, 25, 447
Juhász A. et al., 2010, ApJ, 721, 431
Kaminskii A. A., 1990, Laser Crystals, Their Physics and Properties. Springer-Verlag, Berlin
Karr C., Jr, Kovach J. J., 1969, Appl. Spectrosc., 23, 219
Keller L. P., Thomas K. L., McKay D. S., 1993, Proc. Lunar Planet. Sci. Conf. XXIV, p. 785
Keller L. P., Bradley J. P., Molster F. J., Waters L. B. F. M., Flynn G. J., Henning T., Mutschke H., 2000, Proc. Lunar and Planet. Sci. Conf. XXXI, p. 1860
Keller L. P. et al., 2002, Nat, 417, 148
Keller L. P. et al., 2006, Sci, 314, 1728
Kemper F., Molster F. J., Jaeger C., Waters L. B. F. M., 2002a, A&A, 394, 679
Kemper F., Jaeger C., Waters L. B. F. M., Henning Th., Molster F. J., Barlow M. J., Lim T., de Koter A, 2002b, Nat, 415, 295
Kemper F., Vriend W. J., Tielens A. G. G. M., 2004, ApJ, 609, 826
Kerschbaum F., Posch Th., Nowotny W., 2009, Proc. SPICA Workshop 02004 (doi:10.1051/spica/200903004)
Kimura Y., Kurumada M., Tamura K., Koike C., Chihara H., Kaito C., 2005a, A&A, 442, 507
Kimura Y., Tamura K., Koike C., Chihara H., Kaito C., 2005b, Icarus, 177, 280
Koike Ch. et al., 2006, A&A, 449, 583
Lennie A. R., Vaughan D. J., 1992, Am. Mineral., 77, 1166
Liang W., Whangbo M.-H., 1993, Solid State Commun., 85, 405
Liese H. C., 1974, Appl. Spectrosc., 28, 135
Lisse C. M. et al., 2006, Sci, 313, 635
Lisse C. M., Kraemer K. E., Nuth J. A., Li A. D., Joswiak D., 2007, Icarus, 187, 69
Maldoni M. M., Robinson G., Smith R. G., Duley W. W., Scott A., 1999, MNRAS, 309, 325
Molster F. J., Waters L. B. F. M., 2003, in Henning T. K., ed., Astromineralogy. Springer, New York, p. 121
Molster F. J., Waters L. B. F. M., Tielens A. G. G. M., Koike C., Chihara H., 2002, A&A, 382, 241
Moore M. H., Hudson R. L., 1992, ApJ, 401, 353
Moore M. H., Hudson R. L., 1994, A&AS, 103, 45
Murakami H. et al., 2007, PASJ, 59, S369
Mutschke H., Zeidler S., Posch Th., Kerschbaum F., Baier A., Henning Th., 2008, A&A, 492, 117
Mutschke H., Min M., Tamanai A., 2009, A&A, 504, 12267
Nesvorny D., Jenniskens P., Levison H. F., Bottke W. F., Vokrouhlicky D., Gounelle M., 2010, ApJ, 713, 816
Neugebauer G. et al., 1984, ApJ, 278, L1
Nozaki H., Shibata K., Ohhashi N., 1991, J. Solid State Chem., 91, 306
Nuth J. A., Moseley S. H., Silverberg R. F., Goebel J. H., Moore W. J., 1985, ApJ, 290, L41
Nyquist R. A., Kagel R. O., 1971, Infrared Spectra of Inorganic Compounds (3800-45 cm^{-1}). Academic Press, New York
Pilbratt G. L. et al., 2010, A&A, 518, 14759glp
Posch Th., Mutschke H., Kerschbaum F., Lebzelter Th., 2006, Rev. Mod. Ast., 19, 251
Posch Th., Baier A., Mutschke H., Henning Th., 2007, ApJ, 668, 993

Pring A. et al., 2008, Am. Mineral., 93, 591
Rietmeijer F. J. M., 1989, Proc. Lunar Planet. Sci. Conf. XIX. Cambridge University Press/Lunar and Planetary Institute, Cambridge/Houston, TX, p. 513
Rietmeijer F. J. M., 1993, Proc. Lunar Planet. Sci. Conf. XXIV, p. 1201
Rowan-Robinson M., 2009, Sci, 325, 546
Rubin A. E., 1997, Meteoritics, 32, 231
Soong R., Farmer V. C., 1978, Mineral. Mag., 42, 277
Sunshine J. M. et al., 2006, Sci, 311, 1453
Tomeoka K., Buseck P. R., 1984, Earth Planet. Sci. Lett., 69, 243
Waters L. B. F. M., 2009, SPICA Workshop (2009) 03002, Mineralogy of Circumstellar and Interstellar Dust: The SPICA Potential (doi:10.1051/spica/200903002)
Werner M. W. et al., 2004, ApJS, 154, 1
Westphal A. J., Fakra S. C., Gainsforth Z., Marcus M. A., Ogliore R. C., Butterworth A. L., 2009, ApJ, 694, 18
Whitcomb S. E., Gatley I., Hildebrand R. H., Keene J., Sellgren K., Werner M. W., 1981, ApJ, 246, 416
Wild W. et al., 2009, Exp. Astron., 23, 221
Wincott P. L., Vaughan D. J., 2006, Rev. Mineral. Geochem., 61, 181
Zhang C. Y., Harvey P. M., Smith B. J., Colome C., Difrancesco J., 1994, ApJ, 425, 687
Zolensky M. E., Thomas K. L., 1995, Geochim. Acta, 59, 4707
Zolensky M. E. et al., 2006, Sci, 314, 1735

This paper has been typeset from a TEX/LATEX file prepared by the author.